Contents lists available at ScienceDirect

Journal of Biomechanics

journal homepage: www.elsevier.com/locate/jbiomech

Fusion of video and inertial sensing data via dynamic optimization of a biomechanical model

Owen Pearl [a], Soyong Shin [a], Ashwin Godura [b], Sarah Bergbreiter [a,b], Eni Halilaj [a,c,d,*]

[a] Department of Mechanical Engineering, Carnegie Mellon University, Pittsburgh, PA, USA
[b] Department of Electrical and Computer Engineering, Carnegie Mellon University, Pittsburgh, PA, USA
[c] Department of Biomedical Engineering, Carnegie Mellon University, Pittsburgh, PA, USA
[d] Robotics Institute, Carnegie Mellon University, Pittsburgh, PA, USA

ARTICLE INFO

Keywords:
Kinematics
Inertial measurement units
Computer vision
Direct collocation
Simulation

ABSTRACT

Inertial sensing and computer vision are promising alternatives to traditional optical motion tracking, but until now these data sources have been explored either in isolation or fused via unconstrained optimization, which may not take full advantage of their complementary strengths. By adding physiological plausibility and dynamical robustness to a proposed solution, biomechanical modeling may enable better fusion than unconstrained optimization. To test this hypothesis, we fused video and inertial sensing data via dynamic optimization with a nine degree-of-freedom model and investigated when this approach outperforms video-only, inertial-sensing-only, and unconstrained-fusion methods. We used both experimental and synthetic data that mimicked different ranges of video and inertial measurement unit (IMU) data noise. Fusion with a dynamically constrained model significantly improved estimation of lower-extremity kinematics over the video-only approach and estimation of joint centers over the IMU-only approach. It consistently outperformed single-modality approaches across different noise profiles. When the quality of video data was high and that of inertial data was low, dynamically constrained fusion improved estimation of joint kinematics and joint centers over unconstrained fusion, while unconstrained fusion was advantageous in the opposite scenario. These findings indicate that complementary modalities and techniques can improve motion tracking by clinically meaningful margins and that data quality and computational complexity must be considered when selecting the most appropriate method for a particular application.

1. Introduction

Accessible motion tracking could transform rehabilitation research and therapy. The traditional marker-based approach is limited to specialized laboratories equipped with expensive optical motion tracking systems that require infrared cameras and trained personnel. Inertial sensing and computer vision approaches applied to standard red-green-blue (RGB) videos offer greater flexibility, given their low cost and portability, but collective understanding of the strengths and weaknesses of kinematics estimation algorithms associated with each technology is still evolving (Table 1). Additionally, efforts to merge the strengths of these complementary technologies are sparse.

Vision-based methods using RGB cameras are successful in camera-dense environments, but occlusion continues to pose challenges in reduced-camera settings (Joo et al., 2019). Although now widely used in robotics applications, adoption of vision-based methods in human movement sciences lags behind due to accuracy limitations (Seethapathi et al., 2019). Computer vison models are data-driven and typically not constrained to satisfy physiological constraints. Biomechanical modeling has been considered as a possible approach for improving the accuracy of computer vision approaches and making them more accessible to the biomechanics community (Kanko et al., 2021; Strutzenberger et al., 2021; Uhlrich et al., 2022). Although comparisons with marker-based data suggest that the accuracy of these methods ranges widely between 3–20°, depending on the degree-of-freedom, no study to date has systematically discerned how this accuracy compares to alternative approaches and to what degree the incorporation of biomechanical models improves results.

Similarly, converting multimodal time series data from inertial measurement units (IMU) into accurate joint kinematics remains

* Corresponding author at: Department of Mechanical Engineering, Carnegie Mellon University, 5000 Forbes Ave, Pittsburgh 15213, PA, USA.
E-mail address: ehalilaj@andrew.cmu.edu (E. Halilaj).

https://doi.org/10.1016/j.jbiomech.2023.111617
Accepted 2 May 2023
Available online 6 May 2023

Table 1
Qualitative comparison of state-of-the-art IMU and video-based motion capture techniques for measuring joint kinematics.

Modality	Method	Example Articles	Advantages	Disadvantages
IMUs	Sensor-Fusion Filters (e.g., EKF, Madgwick, Mahoney)	Mahony, 2008. Madgwick, 2010. Sabatini, 2011. Joukov et al., 2014.. Al Borno, 2022.	Computationally efficient; Open-source	Magnetometers are often unreliable; Magnetometer-free approaches are inaccurate
	Deep Learning (e.g., CNNs, LSTMs, Transformers)	Huang, 2018. Rapp, 2021. Mundt, 2020-21. Yi, 2021-22.	Implicitly learns noise; Open-source	Training data are not sufficiently representative of pathologies and activities
	Biomechanical Modeling: Static Optimization	Roetenberg, 2013. Karatsidis, 2016-19.	Predicts GRFs, joint loads, and muscle forces	Requires drift correction using additional sensors; Computational cost; Closed-source
	Biomechanical Modeling: Direct Collocation	Dorschky, 2019.	Predicts GRFs, joint loads, and muscle forces	Requires drift correction via limiting assumptions; Computational cost; Closed-source
Videos	Deep learning & Unconstrained Optimization	Kanazawa, 2018. Iskakov, 2019. Zhang et al., 2020. Kocabas et al., 2020-21.	Computationally efficient; Open-source	Data-driven: training data not representative of clinical populations; Sensitive to occlusions
	Deep Learning & Biomechanical Modeling	Kanko, 2021. Strutzenberger, 2021. Uhlrich, 2022.	Predicts GRFs, joint loads, and muscle forces; Open-source	Data-driven: training data not representative of clinical populations; Computational cost
IMUs & Videos	Deep Learning & Unconstrained Optimization	Halilaj, 2021.	Computationally efficient; Merges complementary modalities; No integration of inertial data necessary	Poor initial estimations from video are propagated in the optimization
	Deep Learning & Dynamically Constrained Optimization	Proposed Method	Predicts GRFs, joint loads, and muscle forces; Merges complementary modalities while satisfying the laws of physics; No integration of inertial data necessary; Accurate with noisy IMU data	Currently, 2-D proof of concept with 3-D validity remaining to be tested; Computational cost

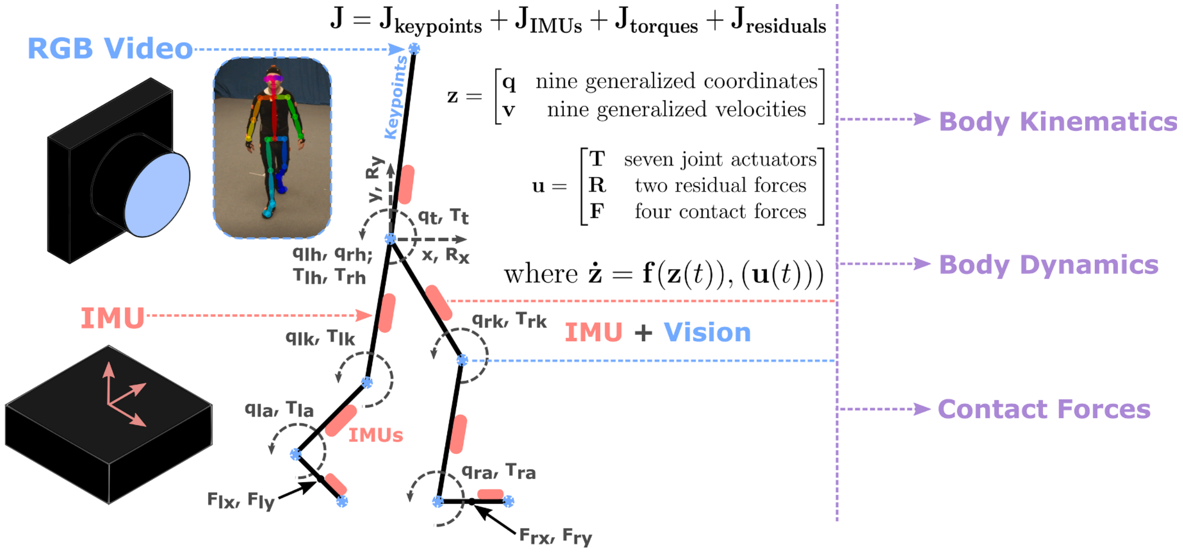
$J = J_{keypoints} + J_{IMUs} + J_{torques} + J_{residuals}$
RGB Video
Keypoints
$z = \begin{bmatrix} q & \text{nine generalized coordinates} \\ v & \text{nine generalized velocities} \end{bmatrix}$
Body Kinematics
y, Ry
$u = \begin{bmatrix} T & \text{seven joint actuators} \\ R & \text{two residual forces} \\ F & \text{four contact forces} \end{bmatrix}$
qt, Tt
x, Rx
qlh, qrh; Tlh, Trh
where $\dot{z} = f(z(t)), (u(t)))$
Body Dynamics
IMU
qrk, Trk
IMU + Vision
qlk, Tlk
qla, Tla
IMUs
Contact Forces
qra, Tra
Flx, Fly
Frx, Fry

Fig. 1. Biomechanical Model and Dynamically Constrained Fusion Overview. Red-green-blue (RGB) video and inertial measurement unit (IMU) data are fused into a single optimal control trajectory tracking problem, where the state of a planar musculoskeletal model is optimized to produce joint center trajectories and inertial profiles that match the experimental data. A nine degree-of-freedom (two translational, seven rotational) model is actuated by seven joint torques, four ground contact forces, and two residual forces accounting for dynamic inconsistencies due to modeling simplifications. The model fuses data from eight anatomical keypoints acquired from three-dimensional triangulation of computer vision keypoints extracted from RGB video data and seven inertial measurement units placed on each rigid body segment. Direct collocation is used to minimize a cost functional with keypoint and IMU tracking error costs and an effort cost for regulating the joint torques and residual forces. (For interpretation of the references to color in this figure legend, the reader is referred to the web version of this article.)

challenging due to the many possible sources of uncertainty, including bias noise, thermo-mechanical white noise, flicker noise, temperature effects, calibration errors, and soft-tissue artifacts (Park & Gao, 2008; Picerno, 2017). Traditional sensor fusion filters used to mitigate drift (Madgwick, 2010; Mahony et al., 2008; Sabatini, 2011) typically rely on magnetometers, which are susceptible to ferromagnetic interference (de Vries et al., 2009). The results of sensor-fusion filters have been refined with biomechanical models (Al Borno et al., 2022), but whether findings will translate to natural environments remains uncertain because marker-based motion capture has been used for sensor-to-body

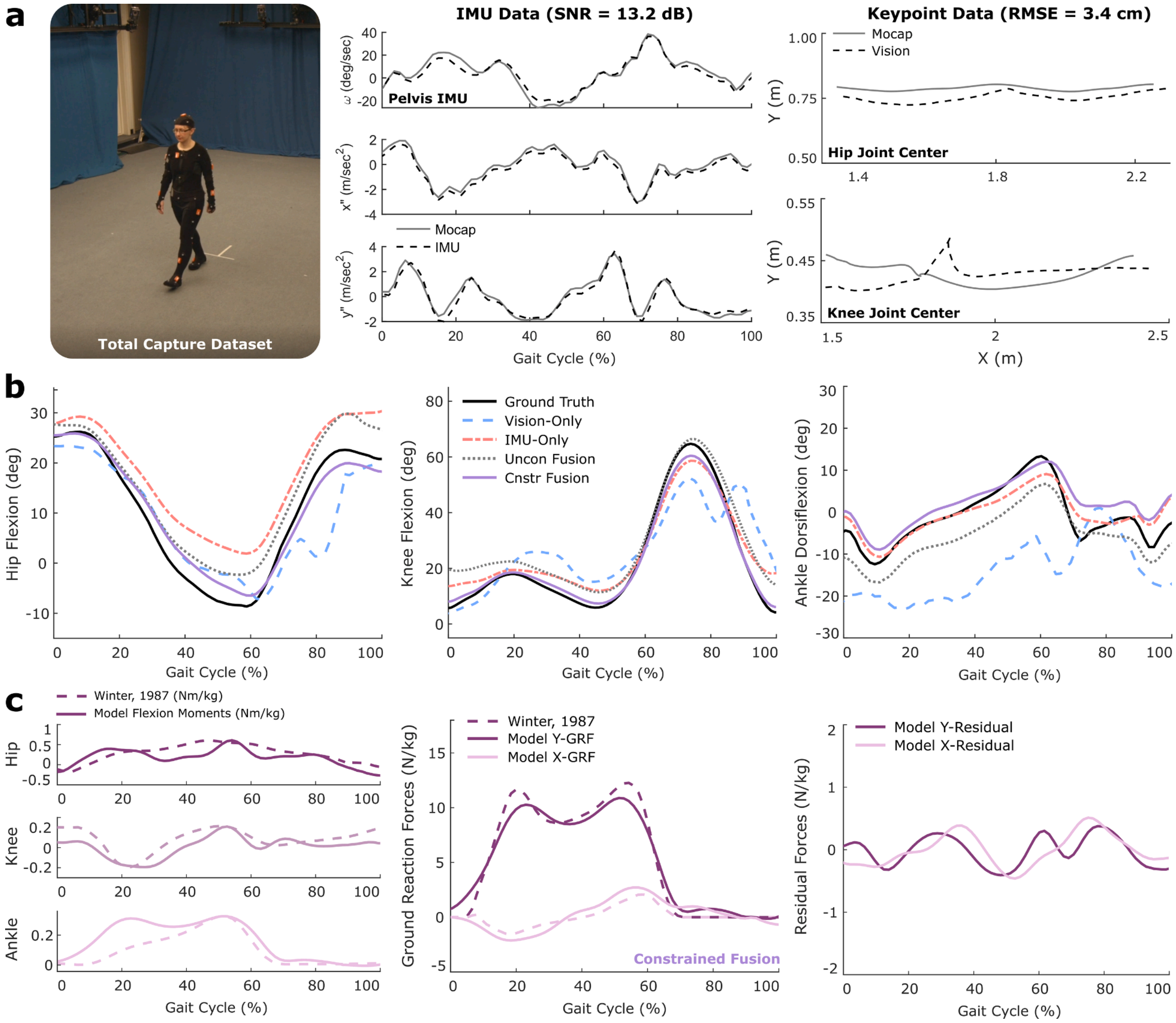

Fig. 2. Experimental Data and the Resulting Markerless Kinematics. (a) We used walking data from 5 subjects recorded with marker-based motion capture, inertial measurement units (IMU), and four videos. The IMU data had a signal-to-noise ratio (SNR) of 13.2 dB, while the video-based keypoints (i.e., joint center positions) had a root-mean-squared error (RMSE) of 3.4 cm. (b) Dynamically constrained fusion of IMU and video data via a biomechanical model and direct collocation (Cnstr Fusion, in solid magenta) improved kinematic predictions over competing markerless motion capture approaches (shown for a single female subject). (c) Although estimation of kinetics was not a study goal, constrained fusion estimated ground reaction forces (middle) and flexion moments (left) relatively well (Winter, 1987). Residual forces (right) are non-physical forces that account for discrepancies between the model and reality when modeling assumptions cause inconsistencies between the biomechanical model and the subject's true multibody dynamics. (For interpretation of the references to color in this figure legend, the reader is referred to the web version of this article.)

calibration and the effect of soft-tissue motion has been mostly eliminated by attaching IMUs to solid marker cluster plates, allowing the IMUs to move rigidly with the marker clusters. Deep learning has been proposed as an alternative (Mundt et al., 2020; Rapp et al., 2021) but has been limited by datasets that are not representative of all activities and clinical populations. Constrained optimization via biomechanical modeling, both static and dynamic, has also been used for estimation of both kinematics and kinetics. Static-optimization approaches rely on zero-velocity detection algorithms from joint constraints, external contacts, and additional sensors (e.g., GPS, RF-based local positioning sensors, barometers) to correct the position of the model at each step (Karatsidis et al., 2019; Roetenberg et al., 2013), while dynamic optimization approaches currently require that the motion be periodic (Dorschky et al., 2019), both of which limit ease of implementation and generalizability.

IMU and vision data have complementary strengths that can be leveraged to overcome their individual limitations, but it is unclear if fusion via a dynamically constrained biomechanical model would improve estimation of kinematics over unconstrained optimization (Halilaj et al., 2021). Inertial sensing can compensate for occlusions in videos, videos can compensate for drift in inertial data, and biomechanical models can add physiological plausibility and dynamical robustness. Here we fuse video and IMU data via dynamic optimization of a nine degree-of-freedom (DOF) model (Fig. 1) and investigate the circumstances under which this approach outperforms (1) standard computer vision techniques using video data, (2) dynamic optimization of a biomechanical model using IMU data, and (3) fusion of IMU and video data via unconstrained optimization (i.e., without a biomechanical model). In addition to comparing these methods using experimental data, we quantified their sensitivity to IMU and video data noise by scaling each subject's unique noise background. We hypothesized that fusion of video and IMU data with biomechanically constrained optimization would improve estimation of kinematics over the alternatives for all of the noise profiles. We have shared a MATLAB library to encourage testing of these techniques with additional data and the exploration of new scientific questions.[1]

2. Methods

2.1. Biomechanical model

To test our leading hypothesis, we used a planar nine DOF biomechanical model that consisted of seven rigid body segments (Fig. 1). One segment represented the head, arms, and torso and three segments represented each leg. Body-segment lengths, masses, and mass moment of inertias were estimated by scaling a three-dimensional musculoskeletal model based on 21 cadavers and 24 young adults (Delp et al., 1990, 2007) with marker-based motion capture data. The model state, z, contained nine generalized coordinates, $\boldsymbol{q}$, and their generalized velocities, $\boldsymbol{v}$, consisting of the horizontal and vertical sagittal plane translation of the pelvis, x and y, and the sagittal plane rotation (flexion–extension angles) of the pelvis, hip joints, knee joints, and ankle joints, q_t, q_{lh}, q_{rh}, q_{lk}, q_{rk}, q_{la}, q_{ra}, respectively:

$$z = \begin{bmatrix} \boldsymbol{q} & \text{gen coords} \\ \boldsymbol{v} & \text{gen velocities} \end{bmatrix},$$

$$\boldsymbol{q} = [x, y, q_t, q_{lh}, q_{rh}, q_{lk}, q_{rk}, q_{la}, q_{ra}]^T.$$

The model control vector, $\boldsymbol{u}$, contained joint torques, $\boldsymbol{T}$, contact forces, $\boldsymbol{F}$, and residual forces accounting for dynamic inconsistencies due to modeling simplifications, $\boldsymbol{R}$ (Fig. 2c). Residual forces are artificial forces applied at the pelvis of the model to help position and orient it in space when real forces alone are insufficient due to modeling simplifications:

$$\boldsymbol{u} = \begin{bmatrix} \boldsymbol{T} & \text{joint torques} \\ \boldsymbol{F} & \text{contact forces} \\ \boldsymbol{R} & \text{residual forces} \end{bmatrix},$$

$$\boldsymbol{T} = [T_t, T_{lh}, T_{rh}, T_{lk}, T_{rk}, T_{la}, T_{ra}]^T,$$

$$\boldsymbol{F} = [F_{lx}, F_{ly}, F_{rx}, F_{ry}]^T,$$

$$\boldsymbol{R} = [R_x, R_y]^T.$$

We used Autolev (Symbolic Dynamics Inc; Sunnyvale, CA) and Kane's equations of motion to derive symbolic expressions for the nine equations of motion in their explicit form and implemented them in MATLAB (Mathworks, Inc; Natick, MA):

$$z' = f(z, \boldsymbol{u})$$

2.2. Experimental data

To test the four markerless approaches for predicting joint kinematics, we used overground walking data from five subjects (4 male; 1 female) from Total Capture (Fig. 2a), a publicly available dataset commonly used to benchmark computer vison methods for motion tracking (Trumble et al., 2017). Motion was captured in a 4 × 6 meter area with eight high definition (HD) RGB video cameras at 60 Hz, seven Xsens IMUs (Xsens; Enschede, The Netherlands) positioned on the pelvis, left and right thigh, left and right shank, left and right foot at 1000 Hz, and a marker-based motion capture system (Vicon Industries, Inc; Hauppauge, NY) at 100 Hz. Sagittal-plane projections of the video and IMU data were used as inputs for the biomechanical model.

2.3. Kinematics Estimation: Vision-Only

We extracted two-dimensional (2-D) keypoints (i.e., joint centers) and the confidence score associated with each keypoint from each RGB video camera using the Cascaded Pyramid Network (CPN) (Chen et al., 2018). We triangulated the keypoints by using a direct linear transformation algorithm to extract three-dimensional (3-D) keypoints (Hartley & Sturm, 1997). Contributions from each video were weighted by the confidence score associated with the corresponding 2-D keypoint. We computed kinematics by minimizing the error between the triangulated keypoints derived from video data and the joint centers of the biomechanical model.

2.4. Kinematics Estimation: Dynamically constrained fusion

Our proposed approach fuses RGB video and IMU data by finding the model states, $z(t)$, and controls, $\boldsymbol{u}(t)$, over time, such that the simulated keypoint locations and body segment accelerations and angular velocities from the model state match those obtained from experimental video and IMU data. This was done by formulating the following optimal control problem and solving it via direct collocation:

$$\begin{array}{ll} \underset{z(t),\boldsymbol{u}(t)}{\text{minimize}} & J(z(t), z'(t), \boldsymbol{u}(t)) \\ \textit{subject to} & z' = f(z, \boldsymbol{u}) \\ & \boldsymbol{x}_L \leq \boldsymbol{x} \leq \boldsymbol{x}_U \\ & \boldsymbol{u}_L \leq \boldsymbol{u} \leq \boldsymbol{u}_U. \end{array}$$

The cost functional $J(z(t), z'(t), \boldsymbol{u}(t))$ is minimized with respect to a bounded state and control and a constraint on the first derivative of the state vector from the explicit form of the equations of motion. The cost functional includes a tracking term for both the keypoints and the inertial data, J_{track}, as well as an effort term for both the joint torque actuators and the residual forces, J_{effort}:

$$J = J_{track} + J_{effort},$$

$$\begin{aligned} J_{track} &= \sum_{i=1}^{n_{keypoint}} \left[\left(x_i^{keypoint} - x_i^{state}\right)^2 + \left(y_i^{keypoint} - y_i^{state}\right)^2 \right] \\ &+ \sum_{j=1}^{n_{IMU}} \left[\left(\ddot{x}_j^{IMU} - \ddot{x}_j^{state}\right)^2 + \left(\ddot{y}_j^{IMU} - \ddot{y}_j^{state}\right)^2 + \left(\omega_j^{IMU} - \omega_j^{state}\right)^2 \right], \end{aligned}$$

$$J_{effort} = \sum_{k=1}^{n_{torques}} (T_k)^2 + \sum_{m=1}^{n_{residuals}} (R_m)^2.$$

We transcribed the large-scale, sparse nonlinear optimization problem via direct collocation using the OptimTraj library for MATLAB (Kelly, 2017).

2.5. Kinematics Estimation: IMU-Only

To perform dynamic optimization with IMU data alone, we took the same steps as in the dynamically constrained fusion approach (2.4) but removed the keypoint terms from within the J_{track} portion of the cost. We followed a previously proposed method and applied the assumption that motion was periodic to overcome the drift resulting from integrating noisy IMU data (Dorschky et al., 2019). This involved segmenting the walking data into individual gait cycles and using the mean gait cycle as the input to the J_{track} term.

2.6. Kinematics Estimation: Unconstrained fusion

For fusion of IMU and video data via unconstrained optimization, we formulated a simplified optimization problem where J_{track} from the IMU and vision optimization was minimized, excluding J_{effort} and constraints on system dynamics and model controls (Halilaj et al., 2021). Here, the optimal set of kinematics was determined by minimizing the error

[1] The code associated with this study is available via SimTK and GitHub.

Table 2
Sources of uncertainty for each modeled IMU signal-to-noise ratio (SNR).

Misplacement (cm)	Misalignment (deg)	Soft-Tissue Motion (cm)	IMU SNR (dB)
0.5	1	0.5	26.7
2.5	5	1.0	17.7
5.0	10	5.0	10.1

between the experimental IMU and video data and the synthetic IMU and keypoint profiles projected from the subject's current state.

2.7. Synthetic data generation

In addition to building simulations with the experimentally captured data, we generated synthetic data to investigate how each of the four approaches responded to changes in noise magnitude. We first estimated the naturally occurring noise background, φ, from the experimental data. Ground-truth-trajectories for each joint center's position and each body segment's accelerations and angular velocities were calculated via marker-based motion capture data and analytic equations formed in Autolev, as noted above. Noise was defined as the difference between the ground-truth trajectories and IMU-based (angular velocity and linear acceleration) or video-based (joint center position) trajectories. We then multiplied this experimental noise background by a scale factor, S, to achieve synthetic data with new noise magnitudes, without editing the shape of the experimentally observed noise distribution:

$$\varphi = data^{exp} - data^{mocap},$$

$$data^{synth} = S\varphi + data^{mocap}.$$

Using marker-based motion capture as the ground truth, the mean ± standard deviation keypoint root-mean-square error (RMSE) for the five subjects was 3.5 ± 0.2 cm. We scaled the naturally occurring noise background, φ, for each subject to RMSEs of 6.0, 3.5, and 1.0 cm by adjusting only the scale of the noise background while maintaining its original distribution. These new noise background magnitudes represented low, medium, and high accuracy conditions, based on single-view and multi-view RGB camera approaches (Iskakov et al., 2019; Kadkhodamohammadi & Padoy, 2019; Kanazawa et al., 2018; Kocabas et al., 2020). An RMSE of 6.0 cm corresponds to single-view approaches such as the Human Mesh Recovery (HMR) (Kanazawa et al., 2018) and Video Inference for Body Pose And Shape Estimation (VIBE) (Kocabas et al., 2020). An RMSE of 3.5 cm corresponds to multi-camera algebraic triangulation approaches such as the one used in this study. An RMSE of 1.0 cm corresponds to multi-camera methods incorporating learnable triangulation, which has acheived state-of-the-art accuracy in computer vision literature (Iskakov et al., 2019; Kadkhodamohammadi & Padoy, 2019). The IMU data had a mean ± standard deviation signal-to-noise ratio (SNR) of 13.2 ± 0.4 dB.

To generate the IMU synthetic data, we scaled the naturally occurring noise background for each subject to SNRs of 10, 17.5, and 25 dB, which represented low, medium, and high IMU accuracy conditions.

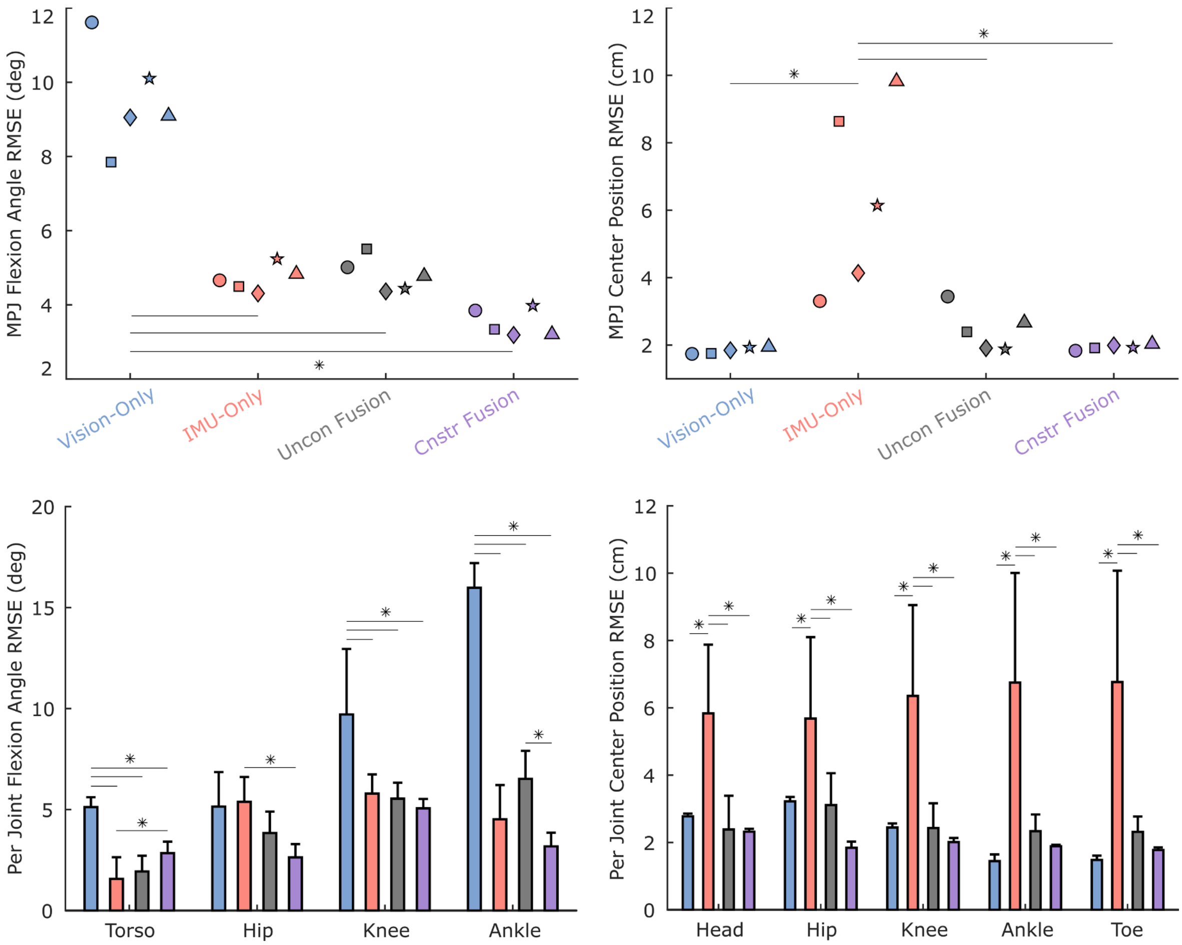

Fig. 3. Comparison of Markerless Approaches. Fusion approaches result in lower mean per joint (MPJ) flexion angle root-mean-square errors (RMSEs) (top left) than the vision-only approach and lower MPJ center position RMSEs (top right) than the IMU-only approach when tested on experimental data from the Total Capture dataset. Each symbol (top plots) represents a unique subject. Fusion methods resulted in better accuracy than single modality methods by maintaining consistent accuracy with respect to both joint angles and joint center positions across all individual joints. (*$p < 0.05$).

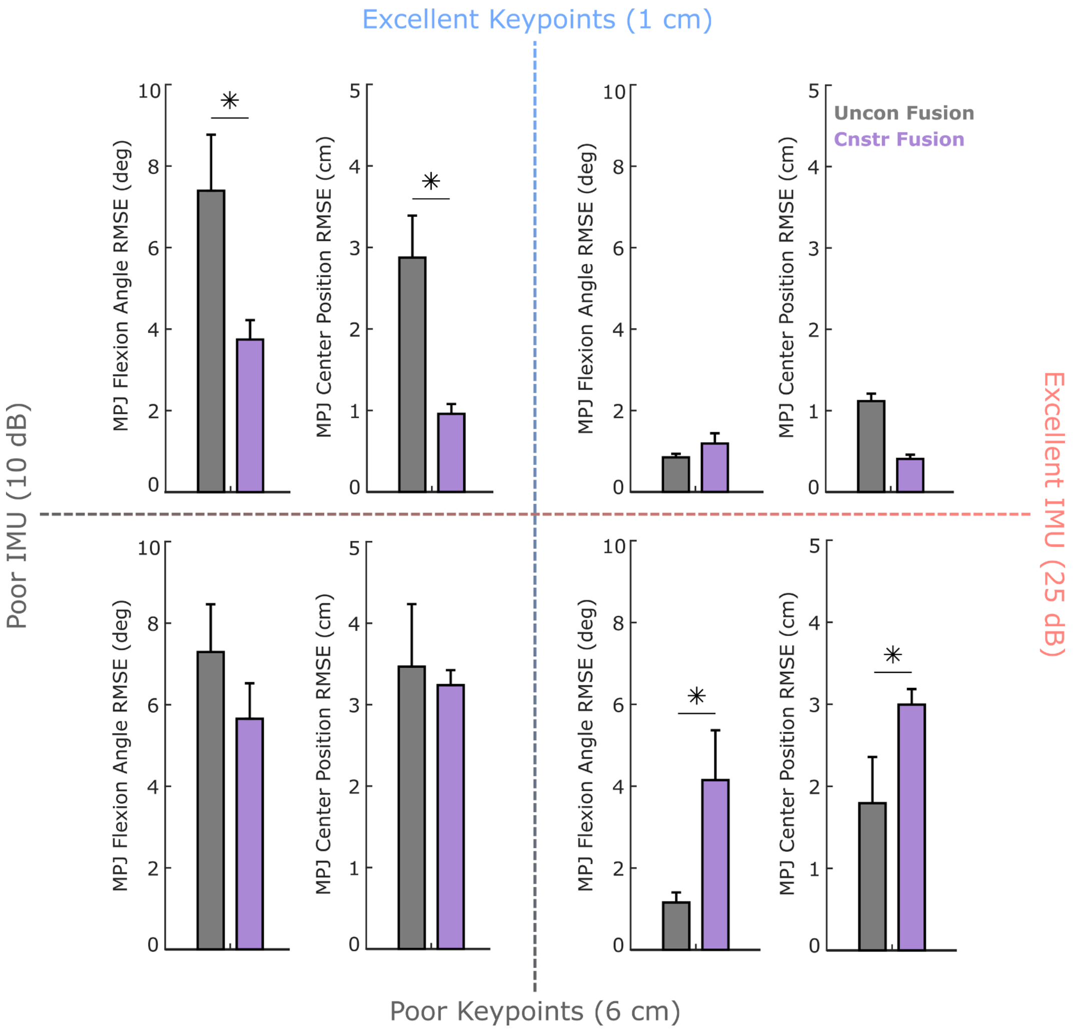

Fig. 4. Sensitivity of Fusion Approaches to Noise. Dynamically constrained fusion was advantageous at lower IMU accuracies and higher keypoint accuracies, whereas unconstrained fusion was advantageous at higher IMU accuracies and lower keypoint accuracies. This phenomenon occurs due to the sometimes complementary, but sometimes redundant nature of IMU data and modeling constraints since both provide information on the first and second order derivatives of the body segment motions. Mean ± standard deviation is plotted here with *p < 0.05.

These conditions corresponded to IMU data influenced by electrical noise in the form of white noise, scale factor noise, and bias nose (Park & Gao, 2008), a range of commonly occurring static misplacement and misorientation errors (Tan et al., 2019), and a range of previously established soft-tissue motion magnitudes naturally occurring during walking (Fiorentino et al., 2017). To determine appropriate magnitudes to which the experimental IMU noise backgrounds would be scaled, we simulated combinations of misplacement, misorientation, and soft-tissue motion artifacts by formulating analytic equations for each body segment's accelerations and angular velocity in Autolev:

$$\boldsymbol{a}_x, \boldsymbol{a}_y, \boldsymbol{\omega}_z = f\left(\boldsymbol{q}, e_{misplacement}, e_{misalignment}, e_{tissue}\right),$$

$$e_{tissue} \sim \mathscr{N}\left(\mu, \sigma^2\right).$$

We added error terms while deriving the body segment inertial profiles to model the static misplacement, $e_{misplacement}$, the static misalignment, $e_{misalignment}$, and the variable misplacement due to soft-tissue motion, e_{tissue}. We calculated the noise background magnitudes corresponding to these errors as the difference between the inertial profiles of the body segments derived with and without incorporating the sources of error, and then scaled the error terms to represent the range of expected naturally occurring noise magnitudes (Table 2). We sampled e_{tissue} from a normal distribution with μ and σ equivalent to the mean and standard deviation of soft-tissue motion magnitudes measured with X-rays (Fiorentino et al., 2017).

2.8. Performance evaluation

We computed mean per joint position error and joint angle error between the simulation results and ground-truth marker-based motion capture data for each optimization approach and noise profile. We used a one-way repeated measures analysis of variance (RM-ANOVA) and Tukey's Honest Significant Difference (HSD) for post-hoc analysis to test the leading hypothesis that dynamically constrained fusion would result in lower kinematic errors compared to the other three approaches. The test was carried out for two primary kinematic outcomes: the mean full-body RMSEs for joint angles and joint center positions. A two-way RM-ANOVA followed by an HSD test within noise conditions was used to test the second hypothesis that dynamically constrained fusion would outperform the other three methods when the data were characterized by different noise profiles. The two-way RM-ANOVA considered both the four competing methods and the nine repeated combinations of IMU and video data noise profiles. Results are presented as mean ± standard deviation of the per-joint RMSE compared to marker-based motion capture. An Anderson-Darling test for normality was used to confirm that the data were normally distributed (Yap & Sim, 2011).

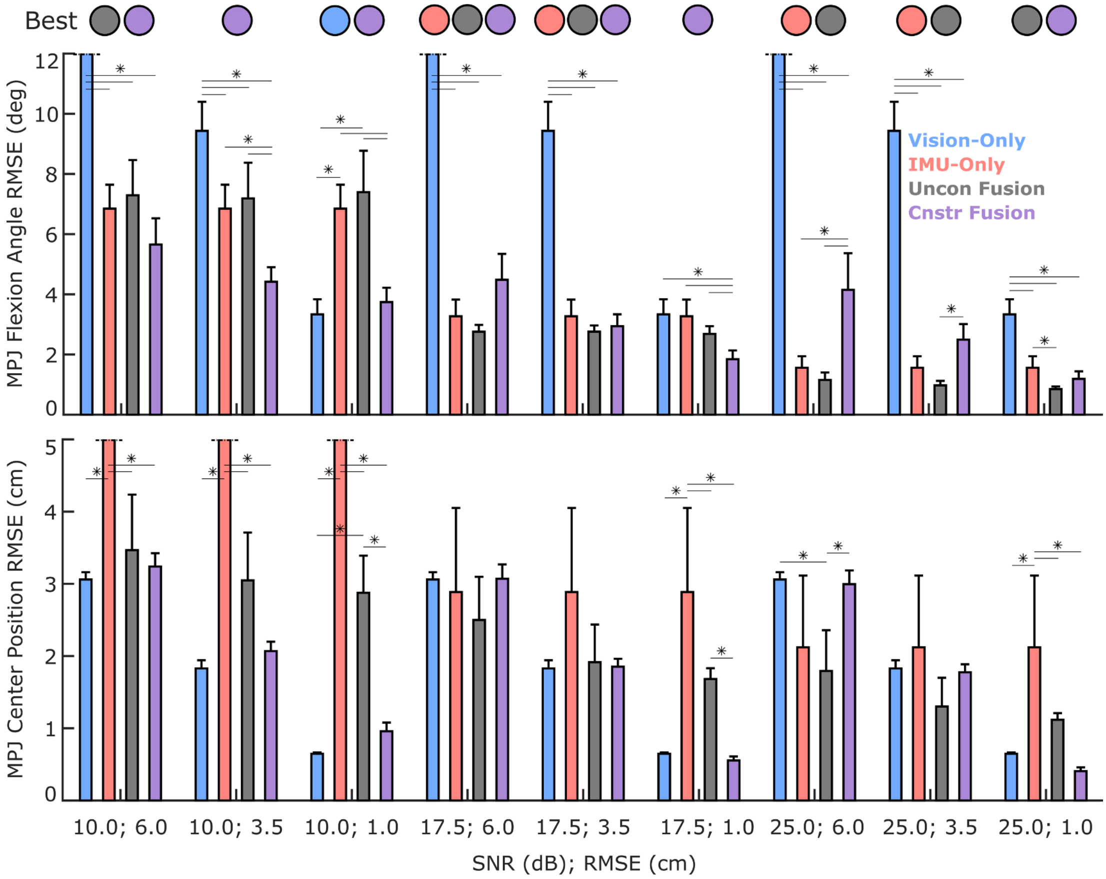

Fig. 5. Sensitivity of Markerless Approaches to Noise. Fusion approaches improve estimation of kinematics over single modality approaches across almost the entire noise spectrum, with few exceptions. Vision-only is consistently outperformed with respect to joint angles, while IMU-only is consistently outperformed with respect to joint center positions. The mean ± standard deviation MPJ flexion angle RMSE (top) and MPJ center position RMSE (bottom) show the difference in kinematics predictions across each noise condition for all four techniques (*$p < 0.05$). The circles indicate which method performed best in each condition, with the color of the circle matching a particular method (blue is vision-only, red is IMU-only, gray is unconstrained fusion, and purple is constrained fusion). In the case of multiple circles, two or more methods performed equivalently. (For interpretation of the references to color in this figure legend, the reader is referred to the web version of this article.)

3. Results

3.1. Comparison of modeling approaches

Dynamically constrained fusion performed better than single-modality methods, but similarly to unconstrained fusion, when using the experimental data (Fig. 2b; Fig. 3). It improved the mean per joint (MPJ) flexion angle RMSE by 6.0° ± 1.2° ($p < 0.0001$) over the vision-only approach and the MPJ center position RMSE by 4.5 ± 2.8 cm ($p = 0.0018$) over the IMU-only approach. Joint flexion angle estimates with the vision-only approach were the least accurate of the four approaches, with RMSEs of 5.1° ± 1.7° for hip flexion, 9.7° ± 3.2° for knee flexion, and 16.0° ± 1.2° for ankle dorsiflexion. Similarly, estimation of joint center positions with the IMU-only approach were the least accurate of the four approaches, producing errors ranging from 5.6 ± 2.4 cm at the hip to 6.8 ± 3.3 cm at the ankle. The two fusion approaches performed similarly to each other and better than single modality approaches by maintaining accuracy with respect to both joint angles and positions. However, dynamically constrained fusion facilitated improvements over unconstrained fusion in estimates of ankle flexion by 3.3° ± 1.3° ($p = 0.0076$).

3.2. Sensitivity to noise

Dynamically constrained fusion performed better than unconstrained fusion when the accuracy of IMU data was low and the accuracy of the video data was high, whereas unconstrained fusion performed better in the opposite scenario (Fig. 4). When the IMU data were of low quality (SNR of 10 dB) and the predicted keypoints from video data were of high quality (RMSE of 1.0 cm), constrained fusion improved the MPJ flexion angle RMSE by 3.7° ± 1.2° ($p < 0.0001$) and the MPJ center position RMSE by 1.9 ± 0.5 cm ($p < 0.0001$) over unconstrained fusion. When the IMU data were of high quality (SNR of 25 dB) and the predicted keypoints were of low quality (RMSE of 6.0 cm), unconstrained fusion improved the MPJ flexion angle RMSE by 3.0° ± 1.4° ($p = 0.0049$) and the MPJ center position RMSE by 1.2 ± 0.7 cm ($p = 0.0183$) over constrained fusion. However, when the quality of IMU data and predicted keypoints was scaled up and down simultaneously, differences between the fusion techniques were not significant.

Single-modality approaches generally performed worse than fusion approaches across the varied data qualities, with some exceptions (Fig. 5). The vision-only approach resulted in significantly worse joint angle estimates than the fusion approaches at every condition except when very low IMU data quality (SNR of 10 dB) was paired with very high keypoint data quality (RMSE of 1 cm). At this condition, vision-only matched constrained fusion ($p = 0.8071$) with an MPJ flexion angle RMSE of 3.3° ± 0.5°. The IMU-only approach resulted in significantly worse MPJ center position RMSEs compared to the fusion approaches at five out of the nine conditions, mainly due to position drift that accumulates over the duration of the IMU-only simulations (Fig. 6). However, at combinations of medium to excellent IMU data accuracy (17.5-25 dB) and poor to medium keypoint data accuracy (6.0-3.5 cm), the

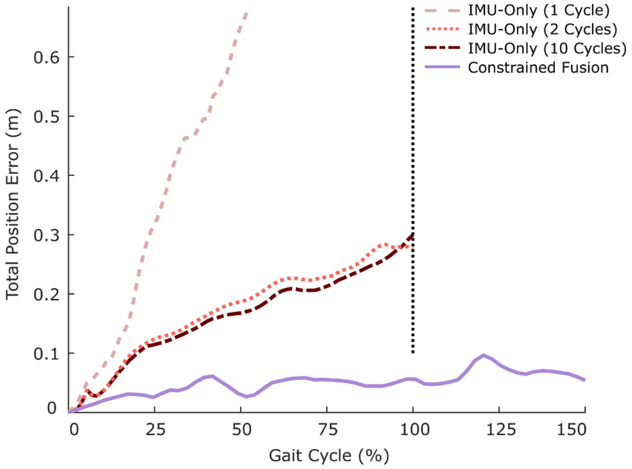

Fig. 6. Error Accumulation of the IMU-Only Method. Observing the full body joint center position error over the gait cycle reveals that dynamically constrained fusion and the other techniques eventually reach an equilibrium error, while IMU-only dynamic optimization continues to accumulate error throughout the simulation duration regardless of the starting IMU data accuracy or the level of denoising. All other approaches can also be run for any arbitrary amount of time, but IMU-only is restricted to complete gait cycles if the periodicity assumption is implemented to reduce drift. However, the rate of error accumulation can be reduced by averaging over multiple periodic gait cycles.

IMU-only approach performed equivalently to fusion methods.

4. Discussion

The complementary strengths of wearable sensing, computer vision, and biomechanical modeling could enhance our ability to capture motion and study gait with greater flexibility and cost-effectiveness than current marker-based approaches. Here, we proposed to fuse RGB video and inertial data with a biomechanical model that simultaneously tracks video and IMU data and investigated when this method improves estimation of kinematics over single-modality methods and unconstrained fusion. We found that fusion of video and inertial data improves kinematics over single-modality methods by achieving high accuracy for both joint angles and joint center positions across all of the tested video and IMU noise backgrounds. We also found that dynamically constrained fusion with a biomechanical model is advantageous over unconstrained fusion when the quality of inertial sensing data is low and the quality of computer vision models is high, whereas unconstrained fusion is advantageous in the opposite case. When the inertial and vision data noise is equally low or equally high, both types of fusion work equally well, but unconstrained is more computationally efficient.

When interpreting these findings, it is important to consider some of the study's limitations. Biomechanical modeling simplifications—reducing degrees of freedom, modeling the head, arms, and torso as a single rigid body, and connecting bones to joints by their end points—can affect the results of simulations. Yet, this simplified approach provides baseline insight on how physics-based modeling can contribute to improvement of IMU-video fusion. Our proof-of-concept study provided a strong premise to continue to invest effort in this direction and expand to 3-D models but do so with better awareness of the scenarios under which such computationally expensive approaches are beneficial. We expect that models with greater complexities and constraints, like OpenSim, will amplify but not overturn the conclusions drawn here. Furthermore, we created synthetic data for testing each approach across different noise magnitudes by simply scaling the noise backgrounds inherent to the experimental IMU and video data. We find this approach elegant and the assumption that the noise distribution remains constant across noise magnitudes more reasonable than making assumptions about that distribution (e.g., Gaussian, uniform), but a validation of the synthetically scaled noise profiles could be used to test that hypothesis in the future. Another limitation is that only walking was considered here. It remains to be determined if the reported findings hold across other activities. As a final note, the video and IMU data may be weighed differently in the cost function based on prior knowledge of their noise profiles, which we did not do. A sensitivity analysis of weights assigned to each modality, however, revealed that this fine-tuning process does not change the results sufficiently to overturn our primary conclusions (Supplementary Fig. 1).

The finding that fusion of RGB video and IMU data is advantageous to single-modality approaches is consistent with findings from other disciplines, despite the lack of exploration in biomechanics. State estimation and simultaneous localization and mapping (SLAM) in autonomous robot navigation is commonly achieved by fusing IMU and video data with extended Kalman filters (Smith et al., 1990) and modified particle filters (Montemerlo et al., 2002). Currently, this fusion method provides the most viable alternative to GPS and lidar-based odometry in aerial navigation (Scaramuzza & Zhang, 2020). IMUs overcome visual SLAM limitations like occlusion, motion blur, lack of visible textures, and inaccurate velocity and acceleration estimates, while videos help enable real-time IMU drift correction (Mirzaei & Roumeliotis, 2008; Nikolic et al., 2014). The complementary nature of videos and IMUs explains why fusion methods consistently outperformed single-modality methods across the entire range of tested noise conditions and why they should be adopted in biomechanics as they are in robot state estimation. In biomechanics, fusion can also help overcome soft-tissue motion artifacts since computer-vision methods detect joint centers where skin motion is small, whereas IMUs sense inertial changes at the middle of body segments where skin motion is non-negligible. However, while fusion is generally better, attention must be paid to both data quality and computational cost to select the most appropriate fusion approach for a particular application.

The overlap between biomechanical models and IMUs causes the unconstrained and biomechanically constrained fusion approaches to diverge under specific noise conditions. Biomechanical models provide mathematical expressions relating applied forces to rigid-body velocities and accelerations. IMUs provide experimental measurements of rigid-body angular velocities and accelerations. When IMU data are inaccurate, adding a model is beneficial because the underlying optimizer can leverage model physics to reduce dependence on suboptimal IMU data. However, when the IMU data are more accurate than the model due to modeling simplifications, adding the model becomes detrimental. Because IMU data quality is limited by miscalibration errors and soft-tissue artifacts, among other sources of noise, the incorporation of a biomechanical model will likely remain beneficial for natural environment applications of fusion methods. Furthermore, incorporation of a model is likely to benefit measurements of faster activities associated with larger skin deformations.

As the prevalence of health monitoring in natural environments increases, so will the frequency with which patients and clinicians are charged with setting up lightweight and portable health-monitoring systems. Markerless motion capture methods must therefore be robust to the IMU and camera noise resulting from suboptimal setups by non-experts. Since fusion of complementary modalities has proven to be more robust to noisy data than single modality methods, we recommend greater emphasis be placed on thoroughly exploring and benchmarking data fusion approaches for biomechanical applications. Our work provides a preliminary comparison of emerging techniques that could make motion capture more accessible. Our findings could help researchers and clinicians make more informed decisions, weighing the required accuracy for a given application against sensor density and computational complexity. Our published code provides an opportunity to further verify our conclusions with real video and IMU data from different laboratories.[1]

CRediT authorship contribution statement

Owen Pearl: Writing – review & editing, Writing – original draft, Visualization, Validation, Software, Methodology, Investigation, Formal analysis, Data curation, Conceptualization. **Soyong Shin:** Writing – review & editing, Investigation, Formal analysis, Data curation. **Ashwin Godura:** Writing – review & editing, Investigation, Formal analysis, Data curation. **Sarah Bergbreiter:** Writing – review & editing, Writing – original draft, Supervision, Conceptualization. **Eni Halilaj:** Writing – review & editing, Writing – original draft, Supervision, Conceptualization.

Declaration of Competing Interest

The authors declare that they have no known competing financial interests or personal relationships that could have appeared to influence the work reported in this paper.

Acknowledgements:

Research reported in this publication was supported by the United States National Science Foundation (NSF) Graduate Research Fellowship Program (award numbers DGE 1745016 and DGE 2140739), a Korean Government Fellowship, and the NSF Disability and Rehabilitation Engineering program (award number CBET 2145473).

Appendix A. Supplementary material

Supplementary data to this article can be found online at https://doi.org/10.1016/j.jbiomech.2023.111617.

References

Al Borno, M., O'Day, J., Ibarra, V., Dunne, J., Seth, A., Habib, A., Ong, C., Hicks, J., Uhlrich, S., Delp, S., 2022. OpenSense: An open-source toolbox for inertial-measurement-unit-based measurement of lower extremity kinematics over long durations. J. Neuroeng. Rehabil. 19 (1), 22. https://doi.org/10.1186/s12984-022-01001-x.

Chen, Y., Wang, Z., Peng, Y., Zhang, Z., Yu, G., & Sun, J. (2018). Cascaded Pyramid Network for Multi-Person Pose Estimation. *ArXiv:1711.07319 [Cs]*. http://arxiv.org/abs/1711.07319.

de Vries, W.H.K., Veeger, H.E.J., Baten, C.T.M., van der Helm, F.C.T., 2009. Magnetic distortion in motion labs, implications for validating inertial magnetic sensors. Gait Posture 29 (4), 535–541. https://doi.org/10.1016/j.gaitpost.2008.12.004.

Delp, S.L., Loan, J.P., Hoy, M.G., Zajac, F.E., Topp, E.L., Rosen, J.M., 1990. An interactive graphics-based model of the lower extremity to study orthopaedic surgical procedures. IEEE Trans. Biomed. Eng. 37 (8), 757–767. https://doi.org/10.1109/10.102791.

Delp, S.L., Anderson, F.C., Arnold, A.S., Loan, P., Habib, A., John, C.T., Guendelman, E., Thelen, D.G., 2007. OpenSim: Open-Source Software to Create and Analyze Dynamic Simulations of Movement. IEEE Trans. Biomed. Eng. 54 (11), 1940–1950. https://doi.org/10.1109/TBME.2007.901024.

Dorschky, E., Nitschke, M., Seifer, A.-K., van den Bogert, A.J., Eskofier, B.M., 2019. Estimation of gait kinematics and kinetics from inertial sensor data using optimal control of musculoskeletal models. J. Biomech. 95, 109278 https://doi.org/10.1016/j.jbiomech.2019.07.022.

Fiorentino, N.M., Atkins, P.R., Kutschke, M.J., Goebel, J.M., Foreman, K.B., Anderson, A. E., 2017. Soft tissue artifact causes significant errors in the calculation of joint angles and range of motion at the hip. Gait Posture 55, 184–190. https://doi.org/10.1016/j.gaitpost.2017.03.033.

Halilaj, E., Shin, S., Rapp, E., Xiang, D., 2021. American Society of Biomechanics Early Career Achievement Award 2020: Toward Portable and Modular Biomechanics Labs: How Video and IMU Fusion Will Change Gait Analysis. J. Biomech. 110650 https://doi.org/10.1016/j.jbiomech.2021.110650.

Hartley, R.I., Sturm, P., 1997. Triangulation. Comput. Vis. Image Underst. 68 (2), 146–157. https://doi.org/10.1006/cviu.1997.0547.

Huang, Y., Kaufmann, M., Aksan, E., Black, M.J., Hilliges, O., Pons-Moll, G., 2018. Deep inertial poser: Learning to reconstruct human pose from sparse inertial measurements in real time. ACM Trans. Graph. 37 (6), 1–15. https://doi.org/10.1145/3272127.3275108.

Iskakov, K., Burkov, E., Lempitsky, V., & Malkov, Y. (2019). Learnable Triangulation of Human Pose. *ArXiv:1905.05754 [Cs]*. http://arxiv.org/abs/1905.05754.

Joo, H., Simon, T., Li, X., Liu, H., Tan, L., Gui, L., Banerjee, S., Godisart, T., Nabbe, B., Matthews, I., Kanade, T., Nobuhara, S., Sheikh, Y., 2019. Panoptic Studio: A Massively Multiview System for Social Interaction Capture. IEEE Trans. Pattern Anal. Mach. Intell. 41 (1), 190–204. https://doi.org/10.1109/TPAMI.2017.2782743.

Joukov, V., Karg, M., Kulic, D., 2014. Online tracking of the lower body joint angles using IMUs for gait rehabilitation. In: 2014 36th Annual International Conference of the IEEEEngineering in Medicine and Biology Society, pp. 2310–2313. https://doi.org/10.1109/EMBC.2014.6944082.

Kadkhodamohammadi, A., & Padoy, N. (2019). *A generalizable approach for multi-view 3D human pose regression* (arXiv:1804.10462). arXiv. http://arxiv.org/abs/1804.10462.

Kanazawa, A., Black, M. J., Jacobs, D. W., & Malik, J. (2018). End-to-end Recovery of Human Shape and Pose. *ArXiv:1712.06584 [Cs]*. http://arxiv.org/abs/1712.06584.

Kanko, R.M., Laende, E.K., Davis, E.M., Selbie, W.S., Deluzio, K.J., 2021. Concurrent assessment of gait kinematics using marker-based and markerless motion capture. J. Biomech. 127, 110665 https://doi.org/10.1016/j.jbiomech.2021.110665.

Karatsidis, A., Bellusci, G., Schepers, H., de Zee, M., Andersen, M., Veltink, P., 2016. Estimation of Ground Reaction Forces and Moments During Gait Using Only Inertial Motion Capture. Sensors 17 (12), 75. https://doi.org/10.3390/s17010075.

Karatsidis, A., Jung, M., Schepers, H. M., Bellusci, G., de Zee, M., Veltink, P. H., & Andersen, M. S. (2018). Predicting kinetics using musculoskeletal modeling and inertial motion capture. *ArXiv:1801.01668 [Physics]*. http://arxiv.org/abs/1801.01668.

Karatsidis, A., Jung, M., Schepers, H.M., Bellusci, G., de Zee, M., Veltink, P.H., Andersen, M.S., 2019. Musculoskeletal model-based inverse dynamic analysis under ambulatory conditions using inertial motion capture. Med. Eng. Phys. 65, 68–77. https://doi.org/10.1016/j.medengphy.2018.12.021.

Kelly, M., 2017. An Introduction to Trajectory Optimization: How to Do Your Own Direct Collocation. SIAM Rev. 59 (4), 849–904. https://doi.org/10.1137/16M1062569.

Kocabas, M., Athanasiou, N., & Black, M. J. (2020). VIBE: Video Inference for Human Body Pose and Shape Estimation. *ArXiv:1912.05656 [Cs]*. http://arxiv.org/abs/1912.05656.

Kocabas, M., Huang, C.-H. P., Hilliges, O., Black, M., 2021. PARE: Part Attention Regressor for 3D Human Body Estimation. In: 2021 IEEE/CVF International Conference on Computer Vision (ICCV, pp. 11107–11117. https://doi.org/10.1109/ICCV48922.2021.01094.

Madgwick, S. O. H. (2010). *An efficient orientation filter for inertial and inertial/magnetic sensor arrays*. 32.

Mahony, R., Hamel, T., Pflimlin, J.-M., 2008. Nonlinear Complementary Filters on the Special Orthogonal Group. IEEE Trans. Autom. Control 53 (5), 1203–1218. https://doi.org/10.1109/TAC.2008.923738.

Mirzaei, F.M., Roumeliotis, S.I., 2008. A Kalman Filter-Based Algorithm for IMU-Camera Calibration: Observability Analysis and Performance Evaluation. IEEE Trans. Rob. 24 (5), 1143–1156. https://doi.org/10.1109/TRO.2008.2004486.

Montemerlo, M., Thrun, S., Koller, D., & Wegbreit, B. (2002). FastSLAM: A Factored Solution to the Simultaneous Localization and Mapping Problem. *AAAI-02 Proceedings*, 6.

Mundt, M., Thomsen, W., Witter, T., Koeppe, A., David, S., Bamer, F., Potthast, W., Markert, B., 2020. Prediction of lower limb joint angles and moments during gait using artificial neural networks. Med. Biol. Eng. Compu. 58 (1), 211–225. https://doi.org/10.1007/s11517-019-02061-3.

Mundt, M., Johnson, W.R., Potthast, W., Markert, B., Mian, A., Alderson, J., 2021. A Comparison of Three Neural Network Approaches for Estimating Joint Angles and Moments from Inertial Measurement Units. Sensors 21 (13), 4535. https://doi.org/10.3390/s21134535.

Nikolic, J., Rehder, J., Burri, M., Gohl, P., Leutenegger, S., Furgale, P.T., Siegwart, R., 2014. A synchronized visual-inertial sensor system with FPGA pre-processing for accurate real-time SLAM. IEEE International Conference on Robotics and Automation (ICRA) 2014, 431–437. https://doi.org/10.1109/ICRA.2014.6906892.

Park, M., Gao, Y., 2008. Error and Performance Analysis of MEMS-based Inertial Sensors with a Low-cost GPS Receiver. Sensors 8 (4), 2240–2261. https://doi.org/10.3390/s8042240.

Picerno, P., 2017. 25 years of lower limb joint kinematics by using inertial and magnetic sensors: A review of methodological approaches. Gait Posture 51, 239–246. https://doi.org/10.1016/j.gaitpost.2016.11.008.

Rapp, E., Shin, S., Thomsen, W., Ferber, R., Halilaj, E., 2021. Estimation of kinematics from inertial measurement units using a combined deep learning and optimization framework. J. Biomech. 116, 110229 https://doi.org/10.1016/j.jbiomech.2021.110229.

Roetenberg, D., Luinge, H., & Slycke, P. (2013). *Xsens MVN: Full 6DOF Human Motion Tracking Using Miniature Inertial Sensors*. 10.

Sabatini, A.M., 2011. Estimating Three-Dimensional Orientation of Human Body Parts by Inertial/Magnetic Sensing. Sensors 11 (2), 1489–1525. https://doi.org/10.3390/s110201489.

Scaramuzza, D., Zhang, Z., 2020. Aerial Robots, Visual-Inertial Odometry of. In: Ang, M. H., Khatib, O., Siciliano, B. (Eds.), Encyclopedia of Robotics. Springer, Berlin Heidelberg, pp. 1–9. https://doi.org/10.1007/978-3-642-41610-1_71-1.

Seethapathi, N., Wang, S., Saluja, R., Blohm, G., & Kording, K. P. (2019). *Movement science needs different pose tracking algorithms* (arXiv:1907.10226). arXiv. http://arxiv.org/abs/1907.10226.

Smith, R., Self, M., Cheeseman, P., 1990. Estimating uncertain spatial relationships in robotics. Autonomous Robot Vehicles.

Strutzenberger, G., Kanko, R., Selbie, S., Schwameder, H., & Deluzio, K. (2021). *ASSESSMENT OF KINEMATIC CMJ DATA USING A DEEP LEARNING ALGORITHM-BASED MARKERLESS MOTION CAPTURE SYSTEM*. 4.

Tan, T., Chiasson, D.P., Hu, H., Shull, P.B., 2019. Influence of IMU position and orientation placement errors on ground reaction force estimation. J. Biomech. 97, 109416 https://doi.org/10.1016/j.jbiomech.2019.109416.

Trumble, M., Gilbert, A., Malleson, C., Hilton, A., Collomosse, J., 2017. Total Capture: 3D Human Pose Estimation Fusing Video and Inertial Sensors. Proc. British Mach. Vis. Conf. 2017, 14. https://doi.org/10.5244/C.31.14.

Uhlrich, S.D., Falisse, A., Kidziński, Ł., Muccini, J., Ko, M., Chaudhari, A.S., Hicks, J.L., Delp, S.L., 2022. *OpenCap: 3D human movement dynamics from smartphone videos* [Preprint]. Bioengineering. https://doi.org/10.1101/2022.07.07.499061.

Winter, D.A., 1987. The biomechanics and motor control of human gait. Univ. of Waterloo Press.

Yap, B.W., Sim, C.H., 2011. Comparisons of various types of normality tests. J. Stat. Comput. Simul. 81 (12), 2141–2155. https://doi.org/10.1080/00949655.2010.520163.

Yi, X., Zhou, Y., & Xu, F. 2021. *TransPose: Real-time 3D Human Translation and Pose Estimation with Six Inertial Sensors* (arXiv:2105.04605). arXiv. http://arxiv.org/abs/2105.04605.

Yi, X., Zhou, Y., Golyanik, V., Habermann, M., Shimada, S., Theobalt, C., & Xu, F. 2022. *Physical Inertial Poser (PIP): Physics-aware Real-time Human Motion Tracking from Sparse Inertial Sensors*. 15.

Zhang, Z., Wang, C., Qin, W., Zeng, W., 2020. Fusing wearable IMUs with multi-view images for human pose estimation: a geometric approach. In: 2020 IEEE/CVF Conference on Computer Vision and Pattern Recognition (CVPR), pp. 2197–2206. https://doi.org/10.1109/CVPR42600.2020.00227.